Chemical Engineering Science 59 (2004) 5249–5259

Chemical Engineering Science

www.elsevier.com/locate/ces

Experimental investigation of Taylor vortex photocatalytic reactor for water purification

Paritam K. Dutta, Ajay K. Ray*

Department of Chemical and Biomolecular Engineering, The National University of Singapore, 10 Kent Ridge Crescent, Singapore 119260, Singapore

Received 17 February 2004; received in revised form 13 May 2004; accepted 4 July 2004
Available online 15 September 2004

Abstract

A Taylor vortex photocatalytic reactor was developed that creates unsteady Taylor–Couette flow in between the two co-axial cylinders by re-circulating fluids form bulk to the inner cylinder wall, which was coated with TiO_2. Systematic investigation for flow development as well as photocatalytic degradation of three different organic compounds was carried out. The effect of Reynolds number and catalyst loading on photocatalytic degradation were compared for both slurry and fixed catalyst system. The experimental results demonstrate that Taylor vortex photocatalytic reactor is promising for water purification even when catalyst is fixed, as there is no significant difference in overall degradation rate between slurry and immobilized systems.
© 2004 Elsevier Ltd. All rights reserved.

Keywords: Catalysis; Chemical reactor; Environment; Pollution; Mixing; Mass transfer; Fluid mechanics; Reaction engineering; Multiphase reactor; Photochemistry; Catalyst activation

1. Introduction

In recent years, semiconductor photocatalysis has received an increasing attention for water purification due to its intriguing advantages over other traditional water purification processes. In this process, low-energy ultraviolet light is used to generate holes and electrons, which oxidizes toxic organic pollutants (Zhou and Ray, 2003) and/or reduces toxic metal ions (Chen and Ray, 2001). Simultaneous removal of organic compounds and metal ions makes this process unique over other process. Degussa P25 TiO_2 is widely used as the photocatalyst since it is very cheap, biologically and chemically inert, nontoxic, and can be used for extended period without substantial loss of activity. In addition, TiO_2 requires low-energy UV-A light ($\lambda < 380\,\text{nm}$), resulting in energy requirements as low as $1–5\,\text{W/m}^2$ of catalyst surface area and can even be activated by sunlight. However, the efficiency of this process is low due to low photon absorption of the catalyst particles and recombination of the photo-generated holes and electrons within the bulk of the material dissipating the input energy as heat.

In the last several years, a large number of research papers have been published based on laboratory studies with promising results over wide range of organic and metal contaminants in water. Despite the appealing results from laboratory-scale studies the development of a practical water treatment system has not yet been achieved (Mukherjee and Ray, 1999). In the design of fixed-bed photocatalytic reactors, one must address two issues, namely, uniform distribution of light and mass transfer of pollutants to the catalytic surface. Earlier our research group did experimental studies on reactors containing catalyst-coated tube bundles (Ray, 1999), catalyst coated extremely narrow diameter immersion-type lamps (Ray and Beenckers, 1998), and catalyst coated rotating tube bundles (Ray, 1998). The experimental as well as simulation results revealed that photocatalytic reaction is primarily diffusion (mass transfer) controlled when catalyst is fixed (Periyathamby and Ray, 1999). The photocatalytic reaction takes place at the

* Corresponding author. Tel.: +65-6874-8049; fax: +65-6779-1936.
E-mail address: cheakr@nus.edu.sg (A.K. Ray).

0009-2509/$ - see front matter © 2004 Elsevier Ltd. All rights reserved.
doi:10.1016/j.ces.2004.07.091

fluid–catalyst interface, and in most cases, the overall rate of reaction is limited to the transfer of pollutants to the catalyst surface. In our earlier studies, we have enhanced mass transfer by increasing mixing through turbulence and/or use of baffles. In this work, a new photocatalytic reactor is designed where increase of degradation rate is achieved through flow instability. We considered unsteady Taylor–Couette flow in between two co-axial cylinders where inner cylinder coated with TiO_2 catalyst is rotated at different speed to achieve the desired instability.

Taylor (1923) at first observed the instability of fluid when the inner cylinder exceeds a critical speed between two co-axial cylinders in his established work. Subsequently, significant research works have been published on the hydrodynamics, transport properties and applications of Taylor–Couette flow. Researchers analyzed the Taylor–Couette vortex flow experimentally, mathematically and by numerical simulation and reported different flow patterns at different speed, shape and size of vortices, role of Taylor vortex on radial mixing, effect of axial flow and axial dispersion in Taylor vortex flow, contribution of Taylor vortices in heat and mass transfer, etc. Till now several practical applications of Taylor vortex flow have been reported in wide range of areas. For example, plug flow reactor (Kataoka et al., 1975; 1995), plant bioreactors (Janes et al., 1987), blood plasmaphoresis devices (Beaudin and Jaffrin, 1989), catalytic chemical reactor (Cohen and Marom, 1991), filtration devices (Holeschovsky and Conney, 1991), homogenous photochemistry (Hiam and Pismen, 1994), etc. Sczechowski et al. (1995), was the first to study experimentally Taylor–Couette flow instability in photocatalytic reactor to enhance the photoefficiency. They observed that when catalyst particles were used as suspension the useful reaction took place only periodically. Taylor–Couette flow allows catalyst particles to get into the continuous periodic illumination since only part of the reactor is illuminated due to optical dense fluid. Vortices created in Taylor–Couette flow move the catalyst particles into and out of the illumination area and thus allow pollutants to come into periodic contact with light and darkness. The residence time of the particles in the illuminated area is thus function of the angular velocity of the re-circulating vortices as well as the size of the vortex. They observed 30% higher photoefficiency at 300 rpm by using an unusually high catalyst loading of 10 g/l. However, slurry system raises the question of separating the sub-micron size catalyst particles after degradation of pollutants. In addition, photoefficiency can only be increased at higher rotation speed and at unusual higher catalyst loading, which might not be feasible in practical application. Based on the above considerations, we have designed a new Taylor vortex photocatalytic reactor (TVR) where the outer surface of the inner cylinder is coated with catalyst and the fluorescent lamp is placed inside of the inner cylinder. The immobilization of catalyst eliminates the need for separation of sub-micron size particles after treatment. Three different model compounds, namely, Orange II dye, Eosin B and Benzoic acid, have been used to observe the overall degradation rate at different Reynolds number in order to determine the influence of kinetic and (external) mass transfer (mixing) on overall photocatalytic reaction rate. In addition, overall degradation rates were compared between slurry and fixed bed systems at specific speed of rotation.

2. Taylor–Couette flow and flow instability

Fluids confined within the annular space of a pair of coaxial cylinders suffer centrifugal instability when the inner cylinder rotates differentially with respect to the outer one. This instability appears as a series of counter rotating vortices in the annular gap. Taylor (1923) in his pioneering work was first to observe experimentally and later quantitatively predicted this instability when the inner cylinder reaches a critical speed. The azimuthal Taylor–Couette flow becomes unstable and is replaced by cellular pattern in which the fluid travels as a series of circumferential toroidial vortices known as Taylor–Couette vortices when the speed of the inner cylinder is increased beyond the critical value. The critical speed of the inner cylinder at the onset of the Taylor instability depends upon the aspect ratio (ratio of length and the annular gap) and the kinematic viscosity of fluid. If the inner cylinder speed is increased further, the flow system exhibits a sequence of time-dependent stable vortex flow regimes as well as complicated patterns in the wide transition region between the laminar Couette flow and the turbulent vortex flow. Kataoka (1986) observed different flow patterns at different rotation speed and reported flow regions as laminar Taylor vortex flow (LTVF), Singly periodic wavy vortex flow (SPWVF), doubly periodic wavy flow (DPWF), weakly turbulent wavy vortex flow (WTWVF), and turbulent vortex flow (TVF). The size and number of the vortices formed depended on the aspect ratio of the cylinder. However, the situation can be different for very short or infinitely long cylinder. Moreover, the effective wavelength depends on the initial and boundary conditions. This has been attributed to the existence of many stable solutions of the governing Navier–Stokes equation for flows far from equilibrium. Coles (1965) investigated systematically the wavy vortex flow and found that there are several distinct stable flow states depending upon the path through which final (steady-state) Reynolds number is reached. This suggests non-uniqueness of the flow pattern or the possibility of existence of multiple solutions.

Rayleigh (1920) was first to deduce the criteria of centrifugal instability where he stated that an inviscid rotating flow is unstable if the energy of the rotating fluid particles decreases radially outward. An unstable condition arises when the outer cylinder is held at stationary and the inner cylinder is rotated, the fluid near the inner cylinder experiences a centrifugal force while the fluid near the outer cylinder experiences the presence of stationary wall. If the rotation is increased further, the centrifugal force overcomes the

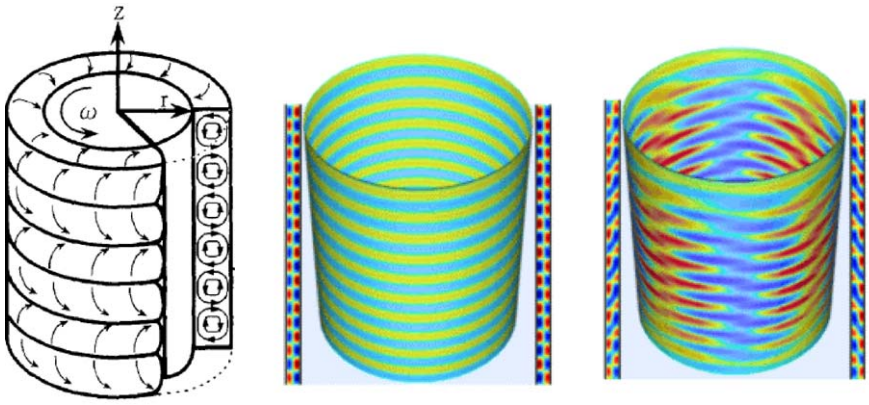

Fig. 1. Flow configuration of Taylor vortices in the annular gap and contours of axial velocity in the annular space from simulation for vertical and cylindrical sections of Taylor–Couette ($Re = 177$) and wavy vortex flow ($Re = 505$).

stabilizing viscous flow and these two opposing forces create instability by creating series of pair of counter rotating vortices where the diameter of an individual vortex is approximately equal to the annular gap. In other words, stability is ensured if

$$\frac{\mathrm{d}}{\mathrm{d}r}[r v_\theta]^2 > 0. \tag{1}$$

According to Taylor (1923), the flow instability is observed when the Taylor number exceeds a critical value where Taylor number is defined by geometrical parameters and the speed of rotation

$$Ta = Re^2 \left[\frac{d}{r_i}\right], \tag{2}$$

where $Re = r_i \omega d/v$. Fig. 1 shows schematic as well as simulated results of the vortex formation and flow patterns in the annular gap between the two co-axial cylinders where the inner cylinder rotates above the critical speed (Sengupta et al., 2001).

3. Mass transfer in Taylor–Couette flow

Taylor–Couette vortex flow between two coaxial cylinders with inner one rotating is of particular interest for the enhancement of mass transfer. In LTVF region, intermixing over cell boundaries is very much suppressed while intra-mixing within cellular vortices is also very weak. SPWVF increases intermixing slightly while DPWVF increases significantly not only intermixing but also intra-mixing. WTWVF has disorganized flow everywhere which greatly enhances both inter and intra mixing, and thus in this region mass transfer resistance within cells is negligible. TVF removes significantly resistance to diffusion of a particular component within cells due to chaotic flow. A considerable number of experimental and theoretical works have been published addressing mass transfer in both laminar and turbulent regions of Taylor vortex flow. Kataoka et al. (1977) experimentally investigated rate of change of heat and mass transfer with Reynolds number on the internal surface of the outer cylinder using electrochemical technique. Gu and Fahidy (1984) measured instantaneous local mass transfer coefficient at the rotating surfaces. Ohmura et al. (1997) investigated effective mass diffusion over cell boundaries using tracer technique. Campero and Vigil (1997) reported axial dispersion at low Reynolds number and its effect on intra vortex mixing. Moore and Conney (1995) calculated the value of axial dispersion coefficient at different Reynolds number and reported values in the range of 0.01–10 cm^2/s, which are several orders of magnitude higher than the molecular diffusion value, and thus, indicate convection within the reactor. Tam and Swinney (1987) measured the value of axial diffusion coefficient using dye injection and found the values of axial diffusion coefficients in the turbulent region of Taylor vortex flow as circa 2 cm^2/s, which is more than five orders of magnitude larger than molecular diffusion coefficients. Hence, turbulent flow in Taylor vortex system can produce an enormous enhancement of mass transport. They also found that effective axial diffusion coefficient (D) value increase monotonically with the increase of Reynolds number and described as $D \alpha Re^{\beta}$ for different radius ratios. They calculated the value of β for radius ratio of 0.73 as 0.75, and for radius ratio of 0.875 as 0.85. Kataoka (1986) correlated the value of mass transfer coefficient with Reynolds number by the following equation:

$$Sh = 6.04\sqrt{R^*}Sc^{0.33}, \tag{3}$$

where, $1 < R^* < 160$, $R^* = Re/Re_c$, $3 \times 10^3 < Sc < 7 \times 10^5$.

Since the Taylor vortex flow can enhance mass transfer significantly, which is the challenge in the present fixed bed photocatalytic reactor; this flow phenomenon was selected in this study.

4. Experimental details

In Fig. 2a, a schematic view of the TVR used in this study is shown, which consists of two coaxial cylinders

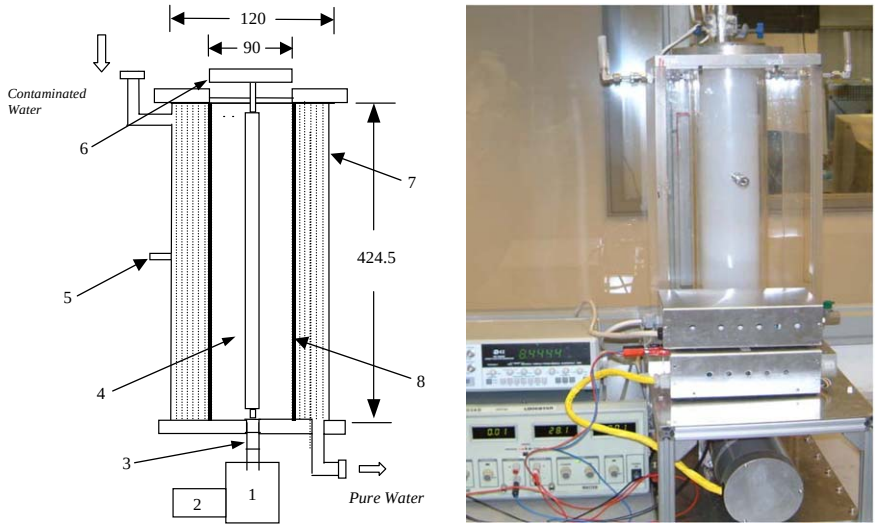

Fig. 2. Experimental setup of Taylor vortex photocatalytic reactor: (1) motor, (2) speed controller, (3) gear coupling, (4) UV lamp, (5) sample collection point, (6) lamp holder, (7) outer cylinder, and (8) catalyst-coated inner cylinder.

(with $r_i/r_o = 0.796$ and aspect ratio, $L/d = 38.24$) made of Perspex in which the inner one rotates while the outer one remains stationary. Perspex is used as it makes it easy for handling and moreover, it can cut off light in UV-B and UV-C ranges, and thereby eliminates direct photolysis of organic compounds. The catalyst was coated on the outer surface of the inner cylinder, which can be rotated at variable speed achieved through gear coupling, a stepper motor together with a frequency generator. A UV lamp (Philips, TLK 40W/10R) was mounted inside of the inner cylinder. The lamp has a spectral distribution energy with a sharp (primary) peak at $\lambda = 365$ nm with an incident light intensity $13\,W/m^2$. The volume of the annular region (in which the reaction liquid is present) is equal to 1.45 l, and the reactor was operated in batch mode. A sampling port was made near the middle portion of the reactor through which samples were collected by a syringe. A UV radiometer (Cole-Parmer Instrument Series 9811) was used to measure the intensity of the light around 365 nm wavelength. The rpm of inner cylinder was determined with a tachometer.

Various visualization fluids (AQ-RF, AQ-1000, ST-1000, AQ-Red Dye) from Kalliroscope Corporation were used to observe the flow pattern in the annular gap. AQ-RF rheoscopic fluid was used as received while AQ-1000 rheoscopic concentrate; ST-1000 bacterial stabilizer and AQ-Red dye were mixed in required proportion to get proper visualization at different speed. Degussa P25 grade TiO_2 was used as photocatalyst as received. The outer surface of the inner cylinder was coated with TiO_2 using a fully automated dip-coating apparatus described elsewhere (Ray and Beenckers, 1998). Varied catalyst film thickness can be obtained by controlling the number of times coated and the speed of coating. Three different model compounds were used in the experiments. Laboratory grade Orange II (Acid orange 7, MW 350.3, dye content 85%) and Eosin B (MW 624.1, dye content 90%) were obtained from Sigma Aldrich Chemical, while Benzoic Acid (MW 122.12, 99.5 + %) was obtained from BDH chemical company. All chemicals were used as received. The overall photocatalytic degradation of the three compounds can be summarized as follow:

$$C_{20}H_6Br_2N_2Na_2O_9 + 19.5O_2 \rightarrow 20CO_2 + NaBr + NaNO_3 + 2H_2O + HBr + HNO_3, \quad (4)$$

$$C_{16}H_{11}N_2O_4SNa + 13O_2 \rightarrow 8CO_2 + NaNO_3 + H_2SO_4 + HNO_3, \quad (5)$$

$$C_6H_5COOH + 8.5O_2 \rightarrow 7CO_2 + 3H_2O. \quad (6)$$

All three model compounds, Orange II, Eosin B and Benzoic acid, have been analyzed by Shimadzu UV-1601PC UV-visible spectrophotometer at wavelength of 485, 518, and 227.8 nm, respectively. A shimadzu 5000A total organic carbon (TOC) analyzer with an ASI-5000 auto-sampler was used to analyze the TOC for all three-model compounds.

The experiments were carried out in two phases. In the first phase, only Taylor–Couette flow development was studied at different speed of rotation (Reynolds number) of the inner cylinder using different flow visualization fluid. Time needed for vortex formation and its movement towards center from both ends, vortex pattern, number of vortices within the reactor length, changes of flow pattern upon increasing the speed of rotation, and the effect of mode of starting (slow or sudden increase) of rotation of the inner cylinder were recorded. In the second phase, photocatalytic degradation experiments were carried out for the three model compounds. All experiments were performed with initial concentration between 20 and 30 ppm and changes in

concentration with time were monitored. In all experiments (slurry as well as fixed catalyst system), about 45 min were allowed to reach adsorption equilibrium before turning on the light for photocatalysis. For slurry system, catalyst particles were removed by syringe driven filter (Millex-HA, 0.45 μm) from the sample before analysis.

5. Results and discussion

5.1. Flow observation

Time-dependent LTVF was observed when the rotation of the inner cylinder exceeds 2.2 rpm ($Re > 111$). The vortex starts at the bottom of the cylinder at the critical Reynolds number and moves toward center of the cylinder with time. The flow was monitored using the Kalliroscope fluid (AQ 1000) and in our system, it took about 12 min to reach steady state as shown in Fig. 3.

At steady state about 21 counter-rotating vortex pairs were observed and the dimension of the each counter-rotating pair was almost twice the gap of the annular space. It was also observed that the outflow boundary is easily distinguishable while the inflow boundary is not so easily distinguishable with bare eye at this critical Reynolds number. When the Reynolds number was increased beyond a secondary critical value of about 228 ($Re/Re_c = 2.05$), Taylor vortex flow takes the shape of azimuthally traveling waves. This wavy vortex flow exists until the Reynolds number reaches about 1770 ($Re/Re_c \approx 16$) at which the flow transforms into turbulent flow. In the turbulent region, we observed at first weakly turbulent vortex flow, which changes to fully turbulent vortex flow at even higher Reynolds number. Fig. 4 shows photographs of the flow patterns at different Reynolds number observed using the flow visualization fluid.

5.2. Computer simulation

Computer simulation was performed to observe the flow pattern within the annular space for the same reactor configuration used in our experimental study. In computing the flow the three-dimensional Navier–Stokes equation was solved in primitive formulation by using the commercial computational fluid dynamics (CFD) software Fluent®. *Time accurate* solution was obtained by solving the governing equations in which no simplification was made regarding symmetry and reflection of the solution. Fluent pre-processor GAMBIT® was used to create geometry and generate grid. The computation of Navier–Stokes equation for Taylor–Couette geometry is expensive. The problem was solved in a mainframe supercomputer (SGI origin 2000). The details of the computational details of simulation runs were reported elsewhere (Sengupta et al., 2001; Kabir and Ray, 2003).

In the first case considered, the Reynolds number is 177, greater than the critical Reynolds number. When the solution was computed, a stable Taylor vortex was realized. Fig. 1 shows the axial velocity at the vertical and cylindrical sections. The cylindrical section lies midway between the inner and outer surfaces. We observe that the solution at this Reynolds number is axisymmetric. At Reynolds number 505 our computations reveal the presence of wavy vortex flow. At this Reynolds number the solution is no longer axisymmetric and involves 3D instabilities. At steady-state condition, 22 pairs of counter-rotating vortices were observed in computer simulation at Reynolds number 505, which is only one pair of vortex more compared with our experimental observation. This slight deviation with the experimental observation might be due to the visualization fluid used in our experiment that was slightly denser and viscous in comparison with pure water considered in the simulation study. Moreover, during computational study at time $t > 0$ impulsive start was assumed whereas in experimental work it requires some finite time to reach the specified speed of rotation.

5.3. Overall reaction rate

Experiments were performed to observe the overall degradation rate of three different model compounds, Orange II dye, Eosin B and Benzoic acid at different Reynolds number in the TVR. The above three model compounds are selected, as their reaction rate constants are an order of magnitude different from each other. The intrinsic reaction rate constant (k_r) of Benzoic acid is circa 13 s^{-1} (Mehrotra et al., 2003), which is higher than Eosin B ($k_r = 0.4\,s^{-1}$) (Zhou and Ray, 2003), which in turn is much higher than Orange II dye ($k_r = 0.017\,s^{-1}$). When the catalyst is immobilized onto a surface, a sequence of events control the overall photocatalytic degradation rate. The pollutant must diffuse from the bulk to the liquid–catalyst interface through a boundary layer, which constitutes the external mass transfer resistance. This is followed by the migration of the pollutant through the porous catalyst layer to find active surface sites where it adsorbs and eventually reacts. Since Degussa P25 TiO_2 is nonporous, inter-particle diffusion is absent and internal mass transfer is only due to intra-particle diffusion within the catalyst particles (Chen et al., 2000). Similar to the diffusion of the pollutant from the bulk to the liquid–catalyst interface, UV light must also reach the catalyst surface to activate the catalyst. The penetration depth of UV light depends on the optical properties of the catalyst and morphology of the catalyst layers.

Fig. 5 shows schematic diagram of the profiles of light intensity and concentration of pollutant in TiO_2 immobilized system used in TVR. The overall reaction rate can be expressed as

$$\frac{1}{k_{\text{obs}}} = \frac{1}{k_{m,\text{ext}}} + \frac{1}{k_{m,\text{int}}} + \frac{1}{k_a} + \frac{1}{k_r}, \tag{7}$$

where k_{obs}, $k_{m,\text{ext}}$, $k_{m,\text{int}}$, k_a, and k_r, are the observed, external and internal mass transfer rates, adsorption and reaction rates, respectively. The external mass transfer resistance can be reduced to a negligible value by increasing mixing in the

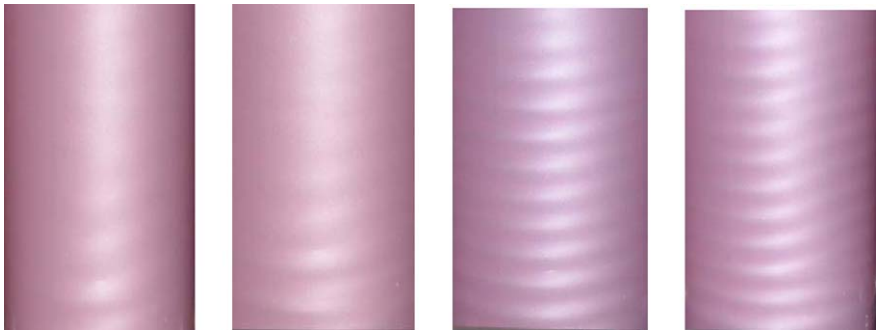

Fig. 3. Progress of time-dependent Taylor vortex flow around critical Reynolds number, $Re_c = 111$.

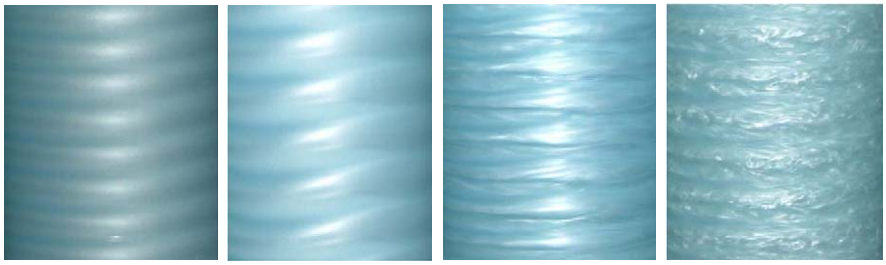

Fig. 4. Photograph of flow pattern at different Reynolds Number. (a) Taylor vortex flow ($Re = 177$), (b) Wavy vortex flow ($Re = 505$), (c) weakly TVF ($Re = 3027$), and (d) TVF ($Re = 8072$).

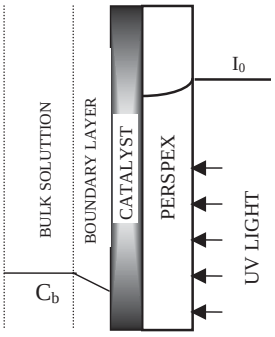

Fig. 5. Schematic diagram of the profiles of UV light intensity and concentration in TiO_2 immobilized system in TVR reactor.

bulk solution, which is created in this work by flow instability whereas increasing light intensity can increase intrinsic reaction rate constant, k_r. But, it is not possible to alter the value of internal mass transfer resistance as it depends on the nature of the catalyst, catalyst coating techniques and morphology of the catalyst layers. Detailed mass transfer analysis in a kinetic reactor has been reported elsewhere (Chen et al., 2000).

5.4. Photocatalytic degradation of pollutants in TVR

Fig. 6a shows photocatalytic degradation of Orange II (Acid orange 7) when experiments were conducted at different Reynolds number. The figure shows that the overall reaction rate increases with the increase of Reynolds number. When there is no rotation ($Re = 0$), the observed rate of degradation is very slow. The increase of photocatalytic reaction rate with Reynolds number demonstrates that external mass transfer controls the overall reaction rate. The observed overall reaction rate is enhanced due to increased mixing due to flow instability within the annular gap of the two co-axial cylinders with the increase of Reynolds number. In the laminar region, mixing is realized but is not significant enough for complete elimination of external mass transfer resistance. Evidently, in turbulent region appreciable enhancement of mixing within the vortices is achieved. Besides mixing, increase of axial dispersion also contribute in enhancement of mass transfer. Many researchers measured and reported the value of axial dispersion in Taylor vortex system, which are several orders of magnitude higher than the molecular diffusion. The value of axial dispersion coefficient is reported to be about five orders of magnitude higher than the molecular diffusion in the turbulent region of Taylor vortex flow (Tam and Swinney, 1987). All these factors contribute to increase in mass transport in the turbulent region. Similar trends were observed for other two model compounds but for brevity, only the rates are compared at two different Reynolds in Fig. 7.

During the process of photodegradation, depending on the model compounds some relatively stable intermediates may be formed, particularly when the parent compounds

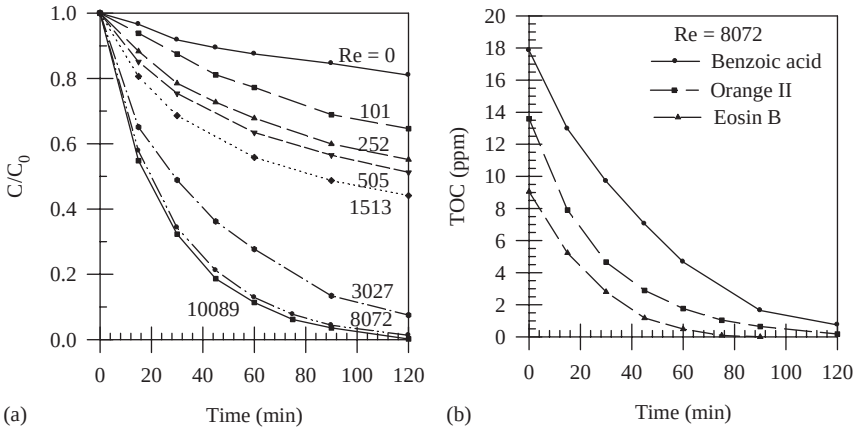

Fig. 6. (a) Photocatalytic degradation rates of Orange II at different Reynolds number. (b) TOC values at $Re = 8072$ for the three-model compounds. Experimental conditions: $C_o = 25\,\text{ppm}$, $I = 13\,\text{W/m}^2$, $\text{TiO}_2 = 0.167\,\text{mg/cm}^2$, and air-equilibrated.

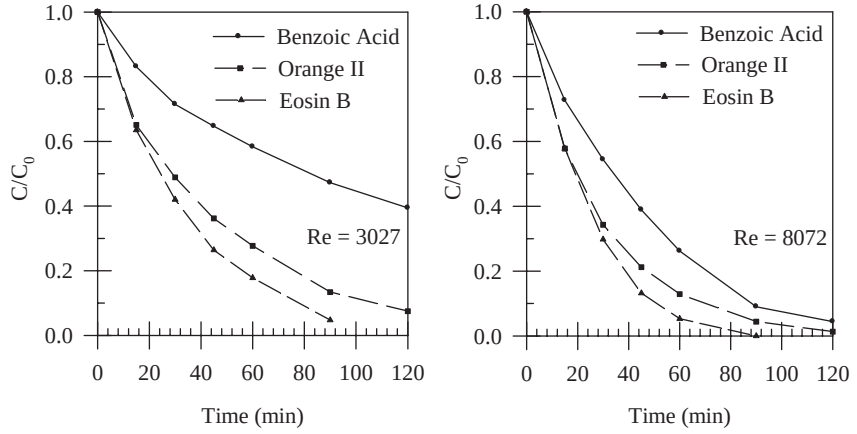

Fig. 7. Comparison of photocatalytic degradation rates of Benzoic acid, Orange II and Eosin B at two different Reynolds number. Experimental conditions: $C_o = 25\,\text{ppm}$, $I = 13\,\text{W/m}^2$, $(\text{TiO}_2) = 0.167\,\text{mg/cm}^2$, and air-equilibrated.

are of large molecular weight, and these intermediates may even be more toxic than the original compound. In view of this, TOC was also measured to make sure that the pollutants have been degraded completely. Fig. 6b shows the TOC value with time for all three-model compounds at Reynolds number 8072, and it is evident from the figure that there is no organic carbon-containing toxic intermediates that is present in the solution after photocatalytic degradation.

Fig. 7 compares photocatalytic degradation rate of the three model compounds at two different Reynolds number. The figure shows that as the Reynolds number is increased from 3027 to 8072, the overall degradation rate is increased implying that external mass transfer resistance decreases with the increase of Reynolds number. A close scrutiny of the figure also reveals that the initial rate for Eosin B and Orange II dye are constant for some time at any particular Reynolds number, and thereafter, the rate of Eosin B degradation (represented as triangle) is faster than Orange dye (represented as square). Moreover, the region of constancy increases with the increase of Reynolds number. This demonstrates that the overall degradation rate of Eosin B and Orange II dye are external mass-transfer controlled, independent of reaction kinetics at least at the beginning. The overall degradation rate is constant at constant mixing although the reaction rate constant of Eosin B ($k_r = 0.4\,\text{s}^{-1}$) is much faster than that of the Orange II dye ($k_r = 0.017\,\text{s}^{-1}$). The overall rate increases only with the increase of mixing. The difference in degradation at later time is probably due to the formation of reaction intermediates, which blocks some of the active catalyst sites. At this later time, the overall rate becomes independent of external mass transfer and is controlled by slow kinetics of the degradation of intermediates. Eosin B with faster reaction rate degrades faster than Orange dye. This is also supported by the experimental results at higher Reynolds number. Enhancement of mixing helps to remove adsorbed intermediates from the catalyst surface increasing available active sites for reaction, and thereby increasing the region of constancy of the overall rate for the two model compounds.

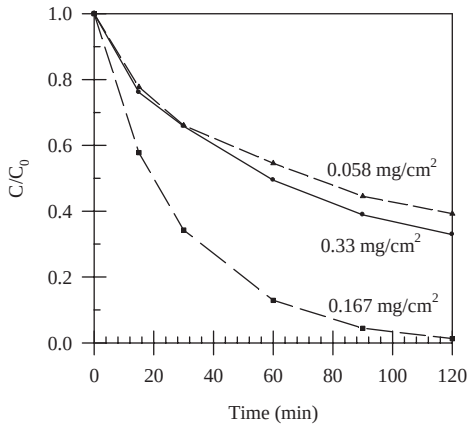

Fig. 8. Comparison of photocatalytic degradation rates of Orange II at different catalyst layer thickness. Experimental conditions: $C_o = 25$ ppm, $I = 13\,W/m^2$, $Re = 8072$, and air-equilibrated.

However, Fig. 7 clearly shows that the degradation rate of Benzoic acid is slower than the other two-model compounds, Orange II and Eosin B, particularly slow at low Reynolds number inspite of the fact that intrinsic reaction rate constant is higher than the other two model compounds. This is due to the fact that adsorption of benzoic acid on TiO_2 is very small (Mehrotra et al., 2003) compared to the other two components, and according to Eq. (7), both adsorption rate and external mass transfer becomes the rate-controlling step. With the increase of mixing, even though the external mass transfer is minimized resulting in the increase of overall rate but the overall rate is still slower than other two model compounds (Eosin B and Orange dye) since the key step controlling the overall rate is the slowest step (highest resistance), which is the adsorption of benzoic acid on the catalyst surface.

5.5. Effect of catalyst layer thickness on degradation rate

Chen et al. (2000) showed both theoretically and experimentally that there exists an optimal catalyst layer thickness for substrate-to-catalyst (SC) illumination. When thin film of catalyst is used, the absorption of light by the catalyst layers will not be strong enough as the wavelength of light used for TiO_2 photocatalysis would be greater than the catalyst layer thickness. On the other hand, when thick catalyst film is used, light might not penetrate the entire catalyst film, and therefore, the catalyst surface in contact with the liquid may not be fully active. The photogenerated holes and electrons generated must diffuse through the increasing number of grain boundaries, which increase the chances of recombination of holes and electrons, and thereby reducing the overall efficiency. Hence, an optimal catalyst layer thickness exists at which the overall reaction rate is at maximum (Chen et al., 2000). Fig. 8 shows the photocatalytic degradation of Orange II for three different catalyst layer thickness. The figure clearly shows that both at higher or at lower catalyst layer thickness, the degradation rate is much slower compared to when the thickness is in between around $0.167\,mg/cm^2$.

5.6. Comparison of slurry and fixed-bed system

In all the previous experimental results reported in this paper, catalyst was immobilized on the outer surface of the inner cylinder. It is expected that when sub-micron size TiO_2 catalyst particles are used as slurry, the external mass transfer limitation would be absent under the experimental conditions. Hence, experiments were conducted with slurry systems to determine to what extent the overall rate is affected compared to when catalyst is immobilized.

Fig. 9 shows photocatalytic degradation of Eosin B at three different Reynolds number when 1 g/l of TiO_2 is used as slurry within the annular gap of the reactor. It was observed that the catalyst particles settle down very fast within the reactor if Reynolds number is maintained below 1510 (30 rpm), and therefore, all experiments were conducted above this Reynolds number. The figure shows that the observed overall initial degradation rate for slurry system is same at low as well as at high Reynolds number. This ascertains that there is no external mass transfer resistance in the slurry system. Although the initial rate is same but as time progresses the figure clearly shows that the degradation rate is slower at low Reynolds number compared to at higher Reynolds number. This is possibly due to at higher Reynolds number (a) the adsorbed intermediates formed during reaction is removed from the catalyst surface due to enhanced mixing, thereby increasing available active sites for further reaction to take place similar to the observation in Fig. 7 for fixed catalyst system, (b) prevents catalyst particles from settling down within the reactor, and (c) catalyst particles are present in less agglomerated form thereby proving more surface area for reaction. Similar trends were observed for Benzoic acid and Orange II dye but are not shown here for brevity.

Fig. 9 (inset) compares the degradation rates between slurry and fixed catalyst system at Reynolds number equal to 8072 at which external mass transfer resistance is minimum for fixed system, while for slurry system, catalyst particles remain suspended without settling down and less opportunity for particle agglomeration. The figure reveals that the degradation rate is marginally faster in slurry system when TiO_2 catalyst loading of 1 g/l is used compared to fixed-bed catalyst system with optimum catalyst loading of $0.167\,mg/cm^2$ for Eosin B. Use of optimal catalyst layer thickness in experiments ensured that catalyst activity at the interface of liquid–solid was high particularly at low UV light intensity of $13\,W/m^2$ compared to slurry system where shielding effect will certainly reduce the overall catalyst activity. The degradation rate in slurry system is expected to be faster compared to fixed catalyst system, as the external mass transfer resistance is negligible. However, it

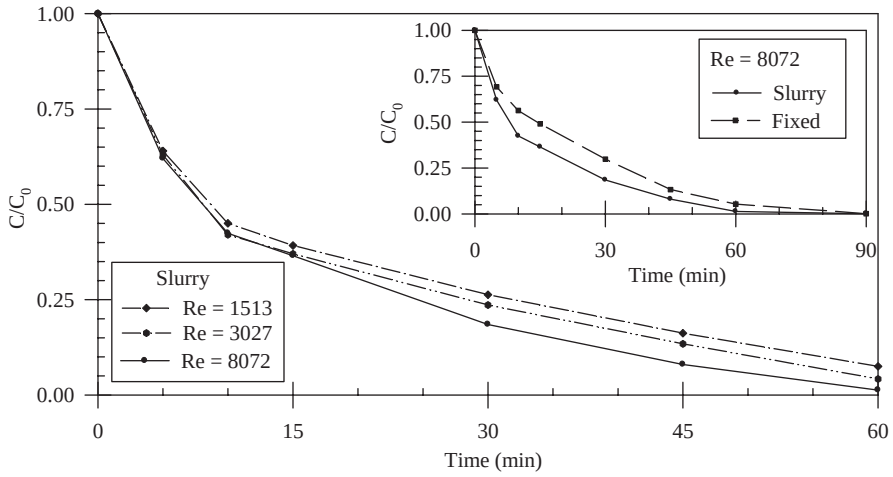

Fig. 9. Photocatalytic degradation rates of Eosin B at different Reynolds number for slurry system. Inset: comparison between slurry and fixed catalyst system at $Re = 8072$. Experimental conditions: $C_o = 25$ ppm, $I = 13\,W/m^2$, $(TiO_2) = 1$ g/l (slurry), and $0.167\,mg/cm^2$ (fixed), and air-equilibrated.

should be noted that when the photocatalyst is being dispersed in the fluid, the useful reaction takes place only periodically when the fluid containing pollutant and suspended catalyst is in contact with the illuminated inner cylinder surface. Sczechowski et al. (1995) reported that for TiO_2 loading of 1 g/l roughly one-quarter of the vortex is illuminated by light while the remaining three-quarters stayed in the dark in their reactor in which annular gap was 1 cm and light intensity used was $30.5\,W/m^2$. They called this as controlled periodic illumination (CPI). They also reported that the photoefficiency increases three-fold when the reactant is illuminated for less than 150 ms, and it stayed in dark for more than 1 s. The maximum photoefficiency achieved by them was 30% at 300 rpm of the inner cylinder when 10 g/l loading of TiO_2 was used. The major problem of achieving higher photoefficiency (apart from the CPI effect) was related to the transport of purified fluid from the vicinity of the catalyst. Moreover, the working fluid is optically dense, and therefore, the light penetration depth is restricted to a distance that is of the order of the boundary layer thickness of the inner cylinder. All these factors lead to lower the degradation rate for the slurry system. When catalyst is immobilized, since CPI effect is absent, one can use a very low level of catalyst loading, and simultaneously, eliminate the process of separation of catalyst particles after purification.

In Table 1, reactor specifications and experimental conditions used and efficiency obtained for the TVR is compared with a slurry reactor (Mehrotra et al., 2003), classical annular reactor (Ray, 1998), multiple tube reactor (Ray, 1999) and tube light reactor (Ray and Beenckers, 1998). When the efficiency of each of the reactors, expressed in terms of 50% pollutant converted per unit time per unit reactor volume per unit electrical power consumed, are compared for the same model component (Orange II dye) with that of a CAR; an increase of about 872% was observed (Table 1). This increase in efficiency was inspite of the fact that the design of this test reactor was far from optimum. In our laboratory-scale reactor, we have used Perspex as material (to avoid breakage), which reduces light intensity significantly. Moreover, the lamp used in this study had UV-A intensity of only $13\,W/m^2$, and the overall rate could be increased significantly if a higher wattage lamp is used. It is apparent that TVR design idea creates great opportunities for building much more efficient photocatalytic reactor.

6. Conclusions

Heterogeneous photocatalysis on semiconductor particles has been shown to be an attractive means for removal of toxic organic, inorganic as well as metal ions from water. Many intriguing advantages exist for immobilized catalyst system compared to slurry system, but earlier experimental as well as simulation studies by our group showed that overall photocatalytic degradation rate is mass transfer controlled when catalyst is fixed. In this work, a new Taylor vortex photocatalytic reactor was designed that creates flow instability to recirculate fluid within the annular gap. The Taylor–Couette flow generated circulates fluids continually between the bulk and the rotating illuminated catalyst coated inner cylindrical surface; thereby minimize the external mass transfer resistance. Detailed experimental as well as simulation study were performed to observe flow pattern at different Reynolds. Subsequently, a comprehensive experimental investigation was carried out with three different model compounds at varied Reynolds number and catalyst loading for both slurry as well as fixed catalyst systems. The experimental results demonstrate that TVR is promising for water purification even when catalyst is fixed, as there is no significant difference in overall degradation rate between slurry and immobilized systems. The enhanced purification was obtained by utilizing fluid dynamical instability

Table 1
Comparison of reactor specifications, experimental conditions, and reactor performance efficiency for photocatalytic decomposition of orange II dye

Photocatalytic reactor	CAR[c]	SR[c]	MTR[d]	TLR[c]	TVR[e]
Volume of reactor (m^3)	3.5×10^{-3}	3.4×10^{-3}	1.2×10^{-3}	5.4×10^{-4}	3.7×10^{-3}
Catalyst surface area (m^2)	0.18	3.7	0.51	0.15	0.12
Parameter k (m^{-1})	69	6139[b]	1087	618	102
Flow rate (m^3/s)	8.4×10^{-5}	Batch operation	3.0×10^{-5}	1.7×10^{-5}	Batch operation
Volume of liquid treated (m^3)	2.6×10^{-3}	6.0×10^{-4}	4.7×10^{-4}	2.4×10^{-3}	1.1×10^{-3}
Electrical energy input (W)	400	960	40	126	40
Efficiency[a] ($s^{-1}m^{-3}W^{-1}$)	9.43×10^{-4}	3.1×10^{-3}	1.18×10^{-2}	1.67×10^{-2}	9.17×10^{-3}
% increase in efficiency	0	229	1157	1668	872

[a]Efficiency is defined as 50% pollutant converted per unit time per unit reactor volume per unit electrical energy used.
[b]The value will be lower than 6139 m^{-1} as all suspended catalyst particles will not be effectively illuminated and the assumption of average particle diameter of 0.3 μm may be too low.
[c]Ray and Beenckers (1998).
[d]Ray (1999).
[e]This work.

associated with centrifugal instability in the cylindrical annular geometry. TVR with immobilized catalyst provides a good opportunity for commercial use as a reactor particularly in obtaining potable water in the developing countries.

Notation

C	concentration, mg/l
CAR	classical annular reactor
d	annular gap between two cylinders, m
D	diffusion
I	intensity, W/m^2
k	rate constant, mass transfer coefficient
L	length of the cylinder, m
MTR	multiple tube reactor
r	radius, m
Re	Reynolds number, $r_i \omega d/v$, dimensionless
Ta	Taylor number, dimensionless
TLR	tube light reactor
Sc	Schmidt number, dimensionless
Sh	Sherwood number, dimensionless
SR	slurry reactor
v	velocity, m/s

Greek letters

ω	angular velocity of inner cylinder, rad/s
v	kinematic viscosity, m^2/s
θ	angular coordinate
λ	light wavelength, (nm)

Subscripts/superscripts

0	initial
*	reduced, dimensionless
c	critical
i	inner
o	outer

Acknowledgements

The author likes to thank Professor T.T. Lim of National University of Singapore and Professor Tapan K. Sengupta of Indian Institute of Technology, Kanpur for their advice and many helpful discussions. The author gratefully acknowledges the financial support provided by the Academic Research Council of National University of Singapore.

References

Beaudin, G., Jaffrin, M.F., 1989. Plasma filtration in Couette flow membrane devices. Artificial Organs 13 (1), 43.
Campero, R.J., Vigil, R.D., 1997. Axial dispersion during low Reynolds number Taylor–Couette flow: intra-vortex mixing effects. Chemical Engineering Science 52, 3303–3310.
Chen, D.W., Ray, A.K., 2001. Removal of toxic metal ions in wastewater by semiconductor photocatalysis. Chemical Engineering Science 56 (4), 1561–1570.
Chen, D.W., Li, F., Ray, A.K., 2000. Effect of mass transfer and catalyst layer thickness on photocatalytic reaction. A.I.Ch.E. Journal 46 (5), 1034–1045.
Cohen, S., Marom, D.M., 1991. Analysis of a rotating annular reactor in the vortex flow regime. Chemical Engineering Science 46 (1), 123–134.
Coles, D., 1965. Transition in circular Couette flow. Journal of Fluid Mechanics 21, 385.
Gu, Z.H., Fahidy, T.Z., 1984. Mass transport in the Taylor-vortex regime of rotating flow. Chemical Engineering Science 40, 1145–1153.
Hiam, D., Pismen, L.M., 1994. Performance of a photochemical reactor in the regime of Taylor–Gortler vortical flow. Chemical Engineering Science 49 (7), 1119–1129.
Holeschovsky, U.B., Conney, C.L., 1991. Quantitative description of ultrafiltration in a rotating filtration device. A.I.Ch.E. Journal 37 (8), 1219.
Janes, D.A., Thomas, N.H., Callow, J.A., 1987. Demonstration of a bubble-free annular—vortex membrane bioreactor for batch culture of red beet cells. Biotechnology Techniques 1 (4), 257.
Kabir, M.F., Ray, A.K., 2003. Performance enhancement of a chemical reactor utilizing flow instability. Journal of Chemical Technology and Biotechnology 78, 314.
Kataoka, K., 1986. Taylor vortices and instabilities in circular Couette flows. In: Cheremisinoff, N.P. (Ed.), Encyclopedia of Fluid Mechanics, vol. 1. Gulf Publishing Company, Houston, pp. 236–274.

Kataoka, K., Doi, H., Hongo, T., Futagawa, M., 1975. Ideal plug-flow properties of Taylor vortex flow. Journal of Chemical Engineering Japan 8, 472–476.

Kataoka, K., Doi, H., Koma, T., 1977. Heat/mass transfer in Taylor vortex flow with constant axial flow rates. International Journal of Heat Mass Transfer 20 (1), 57–64.

Kataoka, K., Ohmura, N., Kouzu, M., Simamura, Y., Okubo, M., 1995. Emulsion polymerization of styrene in a continuous Taylor vortex reactor. Chemical Engineering Science 50 (9), 1409–1416.

Mehrotra, K., Yablonsky, G.S., Ray, A.K., 2003. Kinetic studies of photocatalytic degradation in TiO_2 slurry system: distinguishing working regimes and determining rate dependences. Industrial Engineering and Chemical Research 42 (11), 2273.

Moore, C.M.V., Conney, C.L., 1995. Axial dispersion in Taylor–Couette flow. A.I.Ch.E. Journal 41 (3), 723–727.

Mukherjee, P.S., Ray, A.K., 1999. Major challenges in the design of a large-scale photocatalytic reactor for water treatment. Chemical Engineering Technology 22 (3), 253–260.

Ohmura, N., Kataoka, K., Makino, Y.S.T., 1997. Effective mass diffusion over cell boundaries in Taylor–Couette flow system. Chemical Engineering Science 52 (11), 1757–1765.

Periyathamby, U., Ray, A.K., 1999. Computer simulation of a photocatalytic reactor using distributive computing. Chemical Engineering Technology 22 (10), 881–888.

Ray, A.K., 1998. A new photocatalytic reactor for destruction of toxic water pollutants by advanced oxidation process. Catalysis Today 44, 357–368.

Ray, A.K., 1999. Design, modeling and experimentation of a new large-scale photocatalytic reactor from water treatment. Chemical Engineering Science 54 (16), 3113–3125.

Ray, A.K., Beenckers, A.A.C.M., 1998. A novel photocatalytic reactor for water purification. A.I.Ch.E. Journal 44 (2), 477–483.

Rayleigh, L., 1920. On the Dynamics of Revolving Fluids Scientific Papers, vol. 6. Cambridge, England, pp. 447–453.

Sczechowski, J.G., Koval, C.A., Noble, R.D., 1995. A Taylor vortex reactor for heterogeneous photocatalysis. Chemical Engineering Science 50 (20), 3163–3173.

Sengupta, T.K., Kabir, M.F., Ray, A.K., 2001. A Taylor vortex photocatalytic reactor for water purification. Industrial Engineering and Chemical Research 40 (23), 5268–5281.

Tam, W.Y., Swinney, H.L., 1987. Mass transport in turbulent Couette–Taylor flow. Physical Review A 36 (3), 1374–1381.

Taylor, G.I., 1923. Stability of a viscous liquid contained between two rotating cylinders. Philosophical Transactions Royal Society of London A 223, 289–343.

Zhou, S., Ray, A.K., 2003. Kinetic studies for photocatalytic degradation of Eosin B on thin film of TiO_2. Industrial Engineering and Chemical Research 42, 6020–6033.